Ionic Liquid of a Gold Nanocluster: A Versatile Matrix for Electrochemical Biosensors

Kyuju Kwak, S. Senthil Kumar,[†] Kyunglim Pyo, and Dongil Lee*

Department of Chemistry, Yonsei University, Seoul 120-749, Korea. [†]Present address: Environmental & Analytical Chemistry Division, School of Advanced Sciences, VIT University, Vellore-632014, India.

ABSTRACT Ionic liquids are room-temperature molten salts that are increasingly used in electrochemical devices, such as batteries, fuel cells, and sensors, where their intrinsic ionic conductivity is exploited. Here we demonstrate that combining anionic, redox-active Au_{25} clusters with imidazolium cations leads to a stable ionic liquid possessing both ionic and electronic conductivity. The Au_{25} ionic liquid was found to act as a versatile matrix for amperometric enzyme biosensors toward the detection of glucose. Enzyme electrodes prepared by incorporating glucose oxidase in the Au_{25} ionic liquid show high electrocatalytic activity and substrate affinity. Au_{25} clusters in the electrode were found to act as effective redox mediators as well as electronic conductors determining the detection sensitivity. With the unique electrochemical properties and almost unlimited structural tunability, the ionic liquids of quantum-sized gold clusters may serve as versatile matrices for a variety of electrochemical biosensors.

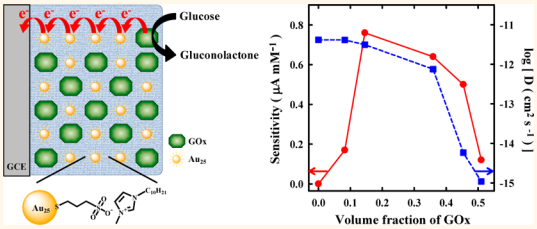

KEYWORDS: gold nanocluster · ionic liquid · biosensor · glucose oxidase · electronic conductivity

In recent years, ionic liquids have received much attention as materials with many practical applications because of promises offered by their unique properties.[1,2] They are typically composed of organic cations (*e.g.*, *N*-alkylpyridinium, *N*,*N*′-dialkylimidazolium) with a variety of anions and exhibit high ionic conductivity, nonflammability, and electrochemical and thermal stability and biocompatibility, making them particularly attractive in the development of electrochemical biodevices that often display long-term instability in the absence of stabilizing matrices.[3] A variety of biosensors and biofuel cells have been developed by immobilizing enzymes in ionic liquid matrices.[4−6] A significant challenge in the development of such devices is to facilitate electron transfer between enzymes and electrodes because the redox center of the enzyme is surrounded by a thick protein layer.[7] Different innovative approaches have been developed to establish electrical communication between the redox center of the enzyme and the electrode by introducing redox mediators or electrical conductors to the ionic liquid matrix.[8−13] Nonetheless, efficient wiring of redox enzymes still remains unaccomplished mostly because of the problems associated with the instability or non-optimal positioning of these electron relays in the heterogeneous mixtures.[12,14] An ideal matrix should immobilize enzymes stably with efficient electrical connection while maintaining their biological activities.[15]

Recent progress in the synthesis and characterization of ligand-protected gold nanoclusters has led to atomically precise gold clusters with definite core numbers (*e.g.*, Au_{25}, Au_{38}, Au_{67}, Au_{102}, and Au_{144}).[16−24] They are highly stable and exhibit unique size-dependent optical, electrochemical, and catalytic properties that differ substantially from their bulk counterpart and represent the bulk-to-molecule transition region.[21−26] Electrochemical and computational investigations have revealed that these molecular clusters display unique redox properties that can be tuned effectively by controlling the core size.[16,21,26] We have recently reported that redox-active Au_{25} clusters can be utilized in electrochemical sensing.[27,28] The Au_{25} clusters entrapped in a silica sol−gel matrix showed excellent electrocatalytic activity toward the oxidation of dopamine, ascorbic

* Address correspondence to dongil@yonsei.ac.kr.

Received for review October 12, 2013 and accepted December 18, 2013.

Published online December 18, 2013
10.1021/nn4053217

acid, and uric acid. Furthermore, the selectivity was found to be dramatically improved by the judicious choice of the capping ligands, showing the great potential for tailored sensing applications.[28]

In this work, we have combined these two unique materials to produce a multifunctioning matrix that can be utilized in a variety of electrochemical applications. An ionic liquid of a quantum-sized gold nanocluster was prepared by ion-pairing of anionic Au_{25} clusters stabilized with (3-mercaptopropyl)sulfonate (MPS-Au_{25}) with 1-decyl-3-methylimidazolium (DMIm) cations. The ion-paired form of Au_{25} (DMIm-Au_{25}) is a highly viscous ionic liquid and readily forms a film on an electrode. Voltammetric investigation has revealed that the Au_{25} film is electrically conductive and the electron transport occurs *via* a diffusion-like electron hopping process.[27,29,30] We demonstrate that DMIm-Au_{25} can be used as an effective matrix for the fabrication of electrochemical glucose biosensors based on glucose oxidase (GOx), the most widely studied assays for the management of diabetes.[31,32] The enzyme electrodes prepared by incorporating GOx in the DMIm-Au_{25} show excellent electrocatalytic activity toward the oxidation of glucose and high glucose binding affinity, demonstrating the great potential of the DMIm-Au_{25} in the development of enzyme-based biosensors.

RESULTS AND DISCUSSION

We recently showed that the water-soluble, anionic MPS-Au_{25} cluster can readily form an ion-pair with hydrophobic counterions such as tetraoctylammonium bromide (TOABr).[33] The strong electrostatic interaction between the sulfonate anion of the MPS ligand and the hydrophobic TOA cation enabled the MPS-Au_{25} cluster to be soluble in organic solvents. Ionic liquids of the Au_{25} cluster can be similarly prepared by ion-pairing MPS-Au_{25} with DMIm cations (see Supporting Information for experimental details). The ion-paired Au_{25} cluster was found to be insoluble in water but soluble in CH_3CN and becomes an ionic liquid when dried. The prepared Au_{25} ionic liquid (DMIm-Au_{25}) was characterized using electrospray ionization (ESI) mass spectrometry. As shown in the negative-mode ESI mass spectrum (Figure 1a), there are peaks observed

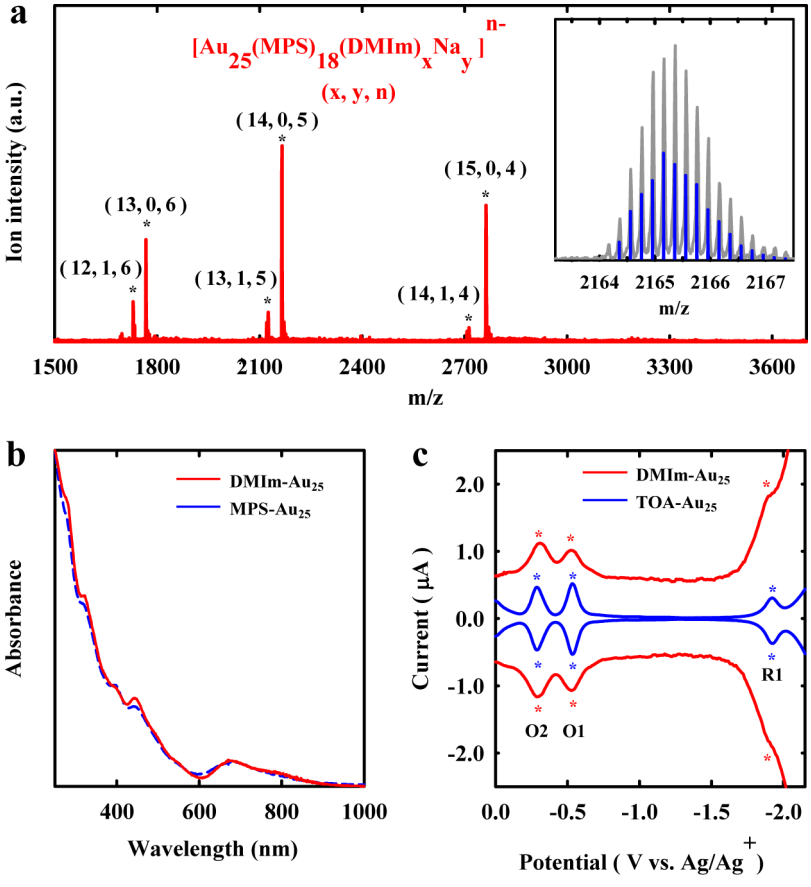

Figure 1. (a) Negative-mode ESI mass spectrum of DMIm-Au_{25}. The assignments coding *x*, *y*, and *n* in parentheses represent the number of $DMIm^+$, Na^+ ions, and charge of cluster anions, respectively. The inset in panel (a) shows a comparison between the experimental data (gray line) and the calculated isotope pattern (blue bars) of $[Au_{25}(MPS)_{18}(DMIm)_{14}]^{5-}$. (b) UV−vis absorption spectra of MPS-Au_{25} and DMIm-Au_{25} in water and CH_3CN. (c) Square wave voltammograms of CH_3CN solution of DMIm-Au_{25} and CH_2Cl_2 solution of TOA-Au_{25} containing 0.1 M Bu_4NPF_6 supporting electrolyte at platinum working electrode. Voltammetric scan was conducted at 60 mV s^{-1} with 20 mV pulse, and the Au_{25} cluster concentrations were ~1.0 mM; ∗ in (a) and (c) indicates the peak positions.

with *m/z* 1500−3000 that represent the cluster ions with overall charge of 6^-, 5^-, and 4^-. These anionic cluster ions are likely generated by the dissociation of DMIm cations. The observed peaks at *m/z* ~2165 Da match well with the isotope pattern of $[Au_{25}(MPS)_{18}(DMIm)_{14}]^{5-}$ as compared in the Figure 1a inset. All the ions observed retain their original cluster composition of $Au_{25}(MPS)_{18}$, and their overall charge is determined by the core charge (−1) and the sum of the counterions ($DMIm^+$ and Na^+) paired with the sulfonate anions.

Figure 1b shows UV−vis absorption spectra of MPS-Au_{25} and DMIm-Au_{25} in water and CH_3CN, respectively. As can be seen in the figure, both spectra are very similar and show the characteristic absorption profile of Au_{25},[34] indicating that DMIm-Au_{25} retains the original optical property of the MPS-Au_{25} cluster after the ion-pairing reaction. Both MPS-Au_{25} and DMIm-Au_{25} display photoluminescence in the near-IR region (~1070 nm) with quantum yields[35] of 0.08 and 0.1%, respectively (Figure S1, Supporting Information). The transmission electron microscopy (TEM) image shown in Figure S2 (Supporting Information) shows that the DMIm-Au_{25} clusters are highly monodisperse with an average size of 1.1 nm. Figure 1c compares square wave voltammograms (SWV) of TOA-Au_{25} and DMIm-Au_{25}. Both ion-paired products of MPS-Au_{25} exhibit the molecule-like redox pattern of Au_{25}.[21,33] TOA-Au_{25} (blue curve) exhibits well-defined oxidation peaks (O1 and O2) at −0.56 and −0.32 V, respectively, and a reduction peak (R1) at −1.96 V *vs* Ag/Ag^+, with an electrochemical HOMO−LUMO gap of 1.40 V. The electrochemical HOMO−LUMO gap is smaller than that typically observed for neutral Au_{25} clusters, presenting the electrostatic field effect of the anionic MPS ligand.[33,36] SWV of DMIm-Au_{25} (red curve) shows similar redox pattern with oxidation peaks at −0.57 and −0.33 V and a reduction peak at around −1.95 V, indicating that the redox behavior of Au_{25} is well-retained in DMIm-Au_{25}. For DMIm-Au_{25}, however, the capacitive background current is significantly larger than that of TOA-Au_{25} presumably due to the modified ionic environment by the imidazolium moiety.

An ionic liquid of Au_{25} is formed when the ion-paired DMIm-Au_{25} is dried. Because the Au_{25} ionic liquid contains sufficient charge carriers, it may be possible to carry out voltammetry in neat (undiluted) DMIm-Au_{25} films. Figure 2a shows the cyclic voltammogram (CV) of the DMIm-Au_{25} film cast on a glassy carbon electrode (GCE) under vacuum. Voltammetry in the DMIm-Au_{25} film shows a pair of well-defined redox peaks with formal potentials at 0.15 and 0.28 V *vs* Ag/AgCl, corresponding to $Au_{25}^{0/1-}$ and $Au_{25}^{1+/0}$

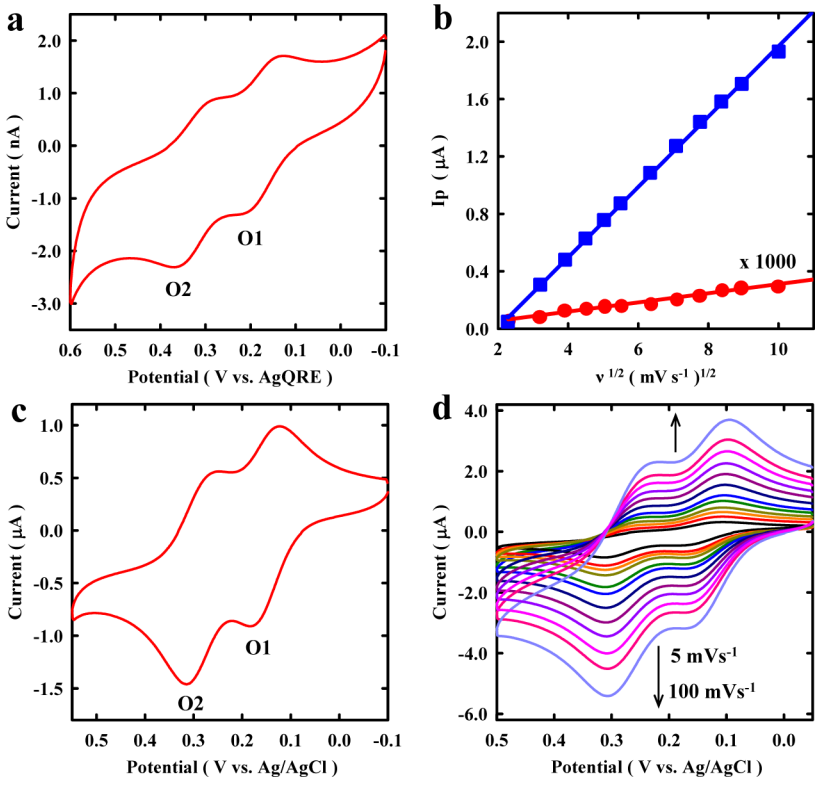

Figure 2. (a) Cyclic voltammogram (CV) of a DMIm-Au_{25} film obtained at scan rate of 20 mV s^{-1} under vacuum. (b) Dependencies of anodic peak (O2) currents (I_p) on the square root of scan rates ($\nu^{1/2}$) obtained from CVs of DMIm-Au_{25} films under vacuum (red circles) and in 0.1 M KCl solution (blue squares), respectively, at varying scan rates (5−100 mV s^{-1}). (c) CV of a DMIm-Au_{25} film obtained at scan rate of 20 mV s^{-1} in 0.1 M KCl solution. (d) CVs of a DMIm-Au_{25} film in 0.1 M KCl solution at varying scan rates (5, 10, 15, 20, 25, 30, 40, 50, 60, 70, 80, and 100 mV s^{-1}). DMIm-Au_{25} films were cast on a glassy carbon electrode.

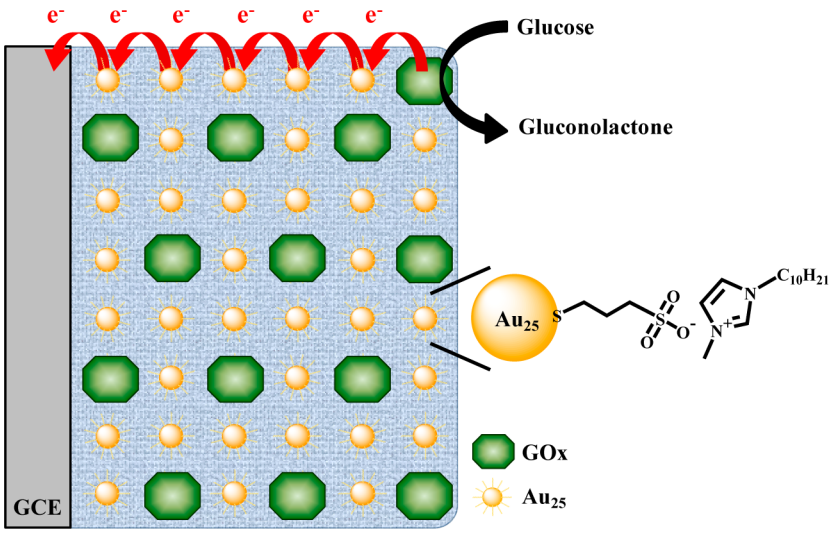

Figure 3. Schematic illustration of processes occurring in a GOx-DMIm-Au_{25} composite electrode. Au_{25}-mediated electrooxidation of glucose-reduced GOx and ensuing electron hopping transport through Au_{25} sites in a GOx-DMIm-Au_{25} composite electrode. The anodic current is proportional to the concentration of glucose, which forms the basis for amperometric detection of glucose.

couples, respectively.[16] That well-resolved voltammetric response obtained even in the absence of any supporting electrolyte reflects the ionically conductive nature of the ionic liquid. The peak currents (I_p) in the voltammograms were found to increase linearly with the square root of scan rate (ν) as can be seen in Figure 2b (red line), indicating a diffusion-controlled redox process.[30] In this highly viscous ionic liquid film, it is expected that the physical diffusivity is negligibly small and thus electron transport predominantly occurs *via* electron hopping (self-exchange) process between Au_{25} cores. Electron hopping process has been observed for Au_{25}-based melt and sol−gel film.[27,29] The electronic diffusion coefficient estimated from the $I_p-\nu^{1/2}$ slope in Figure 2b is very small (1.3×10^{-18} cm^2 s^{-1}), reflecting the rigid nature of the dried DMIm-Au_{25} film.

When the DMIm-Au_{25} film is exposed to aqueous phase (0.1 M KCl), the current response was dramatically increased, as shown in Figure 2c. The DMIm-Au_{25} film is insoluble in water, but it appears to be significantly plasticized by water partitioned into the film. The DMIm-Au_{25} film still retains excellent stability in aqueous solution for voltammetric investigations. As shown in Figure 2c, the voltammogram of DMIm-Au_{25} film exhibits two sets of well-defined redox peaks at the same formal potentials (*i.e.*, 0.15 and 0.28 V) with remarkably enhanced currents. As with the dried film, the peak currents were found to increase linearly with the square root of scan rate, indicating that the redox process is controlled by the electron hopping process between Au_{25} sites.[27] The electronic diffusion coefficient estimated from the $I_p-\nu^{1/2}$ slope in Figure 2b is, however, 4.2×10^{-12} cm^2 s^{-1}, more than 6 orders of magnitude greater than that observed in the dried film. This result suggests that the local mobility of the charge carriers for electron transport in the film is greatly enhanced by contacting with the aqueous phase.

Establishing electrical communication between the redox enzyme and the electrode surface is one of the most challenging tasks in the development of electrochemical biosensors.[7,37] Nanomaterials such as gold nanoparticles and carbon nanotubes have been used for effective electrical wiring of redox enzymes.[13,38,39] The electron transfer properties found in the DMIm-Au_{25} film prompted us to explore the possibility of using it as an electrical communicator between the redox center of enzymes and the electrode. To explore this, we modified GCE with composites prepared by incorporating GOx into the DMIm-Au_{25} film. The composites could be easily prepared by mixing predetermined amount of GOx with MPS-Au_{25} in 2:1 (v/v) CH_3CN/H_2O and then ion-pairing with DMIm cations to form a GOx-DMIm-Au_{25} composite. GOx carries negative charge (isoelectric point ~4.2)[40] in neutral pH and thus can readily pair with DMIm cation along with anionic MPS-Au_{25} clusters. Figure 3 illustrates a modified electrode fabricated by casting the GOx-DMIm-Au_{25} composite on a GCE.

Figure 4a shows CVs of a GOx-DMIm-Au_{25} composite electrode upon the addition of glucose. The composite electrode displays the characteristic voltammetric pattern of Au_{25} clusters, and more importantly, current response increases significantly upon the addition of glucose, indicating the electrocatalytic activity of the composite electrode toward the oxidation of glucose. It is well-known that the enzymatic activity is dependent on pH.[41] Accordingly, the voltammetric response of the GOx-DMIm-Au_{25} electrode was investigated in the pH range from 4 to 8, and the results are shown in Figure S3 (Supporting Information). As can be seen

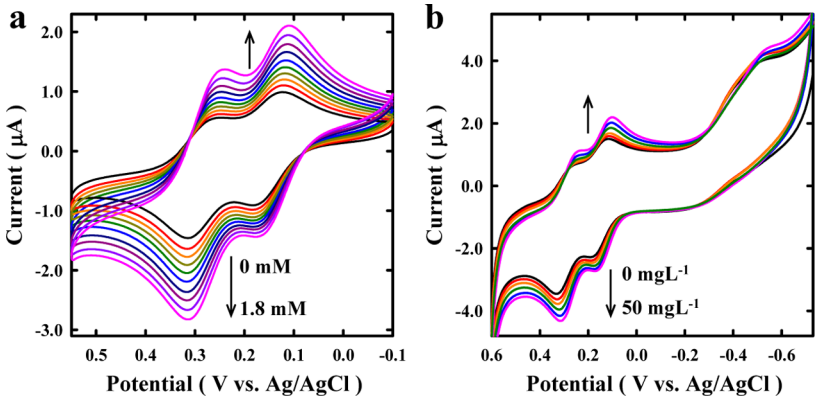

Figure 4. (a) CVs demonstrating the amperometric detection of glucose in concentration range of 0−1.8 mM using a GOx-DMIm-Au_{25} composite electrode (GOx volume fraction = 0.15). (b) CVs demonstrating the Au_{25}-mediated electro-oxidation of electrochemically reduced GOx at a DMIm-Au_{25} electrode in the presence of 0, 10, 20, 30, 40, and 50 mg L^{-1} of GOx. All voltammograms were obtained in PBS (pH 7) containing 0.1 M KCl at 20 mV s^{-1}.

in the figures, the GOx-DMIm-Au_{25} electrodes exhibit linear response to the glucose added in all pH ranges studied. However, maximum sensitivity was observed at pH 7, as expected for GOx-based biosensors,[31] and therefore, all electrochemical measurements of the GOx-DMIm-Au_{25} were carried out at pH 7 using 0.1 M phosphate buffer solution (PBS).

In Figure 4a, the current increase at the formal potentials of Au_{25} undoubtedly manifests the Au_{25}-mediated electro-oxidation of glucose-reduced GOx. It is well-documented that the rate of GOx electro-oxidation is very slow because the cofactor of GOx, flavin adenine dinucleotide (FAD), is buried inside GOx. However, the rate has been found to be greatly enhanced in the presence of redox mediators, such as ferrocene derivatives, ferricyanide, and osmium complexes.[31] The role of Au_{25} in this electrocatalytic reaction can be understood similarly by the following reactions:

$$Au_{25}(red) \rightarrow Au_{25}(ox) \quad (1)$$

$$\text{glucose} + GOx(FAD) \rightarrow \text{gluconolactone} + GOx(FADH_2) \quad (2)$$

$$GOx(FADH_2) + Au_{25}(ox) \rightarrow GOx(FAD) + Au_{25}(red) \quad (3)$$

When appropriate potential is applied, Au_{25} is first oxidized at the electrode (reaction 1). In the presence of glucose, GOx(FAD) generates gluconolactone while it is reduced (reaction 2). The reduced GOx($FADH_2$) is electrocatalytically oxidized to GOx(FAD) by the oxidized Au_{25}, regenerating Au_{25}(red) (reaction 3). These reactions occur in a cycle as long as the analyte (glucose) is available at the electrode surface, resulting in the increase in anodic current from Au_{25} oxidation. The Au_{25}-mediated electro-oxidation of glucose-reduced GOx and ensuing electron transport in the composite electrode is depicted in Figure 3. The increase in anodic peak current varies linearly with the concentration of glucose added, which forms the basis for the amperometric sensing of glucose. The linear range and sensitivity for the determination of glucose were found to be 0.028 to 2.0 mM and 0.76 μA mM^{-1}, respectively. These values obtained at this low potential (0.31 V) compare well with those recently reported for glucose biosensors.[42−44]

To further confirm the mediated electrocatalytic activity of Au_{25}, CVs of the DMIm-Au_{25} film containing no GOx were recorded upon the addition of GOx in the absence of glucose. As can be observed in Figure 4b, the current response of Au_{25} increases linearly with the addition of GOx, suggesting strong electronic communication between Au_{25} and GOx. Both anodic and cathodic currents of Au_{25} were found to increase with the addition of GOx, indicating that the mediated electrocatalytic reaction of Au_{25} is reversible. We note that in the absence of glucose the current increase was only observed when potential was swept from −0.7 V, but no increase was found with sweeping potential from −0.1 V. This result suggests that the FAD cofactor has to be reduced first chemically (by glucose) or electrochemically to observe the current increase. In addition, Figure 4b shows no discernible redox peak of the cofactor (FAD/$FADH_2$) or any increase with the addition of GOx, suggesting that the direct electron transfer[13,37] between GOx and the electrode is insignificant. It has been found that thiolate-protected gold nanoclusters such as Au_{38}, Au_{67}, and Au_{144} exhibit size-dependent redox properties.[16,19] It will be of interest therefore to investigate the size-dependent electrocatalytic activity of these clusters in the future.

The above results attest that Au_{25} in the GOx-DMIm-Au_{25} composite film acts as a redox mediator as well as an electronic conductor. It is of interest, therefore, to determine the optimum fraction of GOx in the GOx-DMIm-Au_{25} composite. The volume fraction of GOx can be easily controlled in the range between 0.083 and 0.51 by varying the amount of GOx in the CH_3CN/H_2O

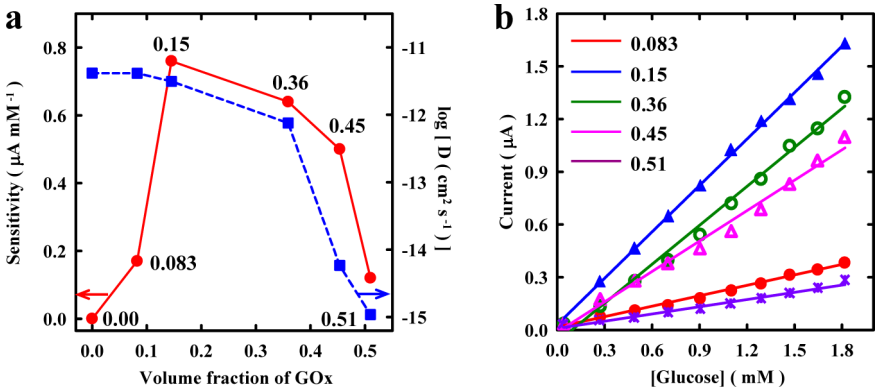

Figure 5. (a) Dependencies of electronic diffusion coefficient (blue) and sensitivity of determination for glucose (red) on the GOx volume fraction. (b) Calibration graphs for the determination of glucose from CVs of GOx-DMIm-Au_{25} composite electrodes with different GOx volume fractions of 0.083, 0.15, 0.36, 0.45, and 0.51.

solution before pairing with DMIm cations (see Materials and Methods). As can be seen in Figure S4 (Supporting Information), all composites display well-resolved, two oxidation waves of Au_{25}, but the current response decreases considerably with increasing GOx fraction. Again, the voltammetric currents of the composites were linearly dependent upon the square root of scan rate, as shown in Figure S5 (Supporting Information). The diffusion coefficients determined from the $I_p-\nu^{1/2}$ slopes are plotted as a function of the GOx volume fraction in Figure 5a. The electronic diffusion coefficient in the DMIm-Au_{25} film, that is, without GOx, is the highest and gradually decreases with increasing GOx fraction up to the fraction of 0.36. Above this fraction, however, the diffusion coefficient drastically drops as the GOx fraction increases to 0.45. This behavior can be understood by the electrical percolation theory which is typically observed in a composite of conductor and insulator.[45,46] In Figure 5a, the volume fraction of ~0.36 appears to correspond to the electrical percolation threshold.

Because the electronic conductivity in the composite film depends on the GOx fraction, it is of interest to inquire into the correlation between the sensitivity and conductivity. The calibration graphs for the determination of glucose for composite films with different GOx fractions are shown in Figure 5b, and the sensitivity values are plotted as a function of the GOx volume fraction in Figure 5a. As can be seen in the figure, the sensitivity is very low at low fraction of GOx simply because of the limited availability of GOx in the film. The sensitivity reaches a maximum at the volume fraction of 0.15. Interestingly, the sensitivity also drops sharply above 0.36, exhibiting the same propensity as the electronic diffusivity. This result confirms that the sensitivity is predominantly controlled by the electronic conductivity in the high GOx-loaded film.

Ionic liquids have proven to be highly biocompatible and been used as a binder for many redox proteins in the fabrication of modified electrodes.[47,48] The ionic liquid film where the proteins are entrapped provides an excellent microenvironment for the proteins to retain their biocatalytic activity. We next evaluate the biocompatibility of Au_{25} ionic liquids for supporting GOx. For comparison, a modified electrode was fabricated by casting an ionic liquid composite containing only GOx (GOx-DMIm), and chronoamperometric response was monitored upon the addition of glucose (red line, Figure 6a). Because there is no Au_{25} in the film, measurable anodic current in the presence of oxygen is only observed at higher overpotentials (see Figure S6a, Supporting Information). The sensitivity of determination for the GOx-DMIm film was determined to be 0.21 μA mM^{-1} at 0.5 V. When Au_{25} clusters are present in the film, the sensitivity is greatly enhanced and the anodic current is observed at much lower potential (0.31 V). The sensitivities determined from the plots in Figure 6a (and calibration graphs in Figure S6b, Supporting Information) for GOx-DMIm-Au_{25} with GOx fractions of 0.15 and 0.45 are 0.85 and 0.43 μA mM^{-1}, respectively.

Finally, the enzyme–substrate binding kinetics was compared for the GOx-DMIm and GOx-DMIm-Au_{25} electrodes. Figure 6b shows the Lineweaver–Burk plot,[49] that is, double reciprocal plots of the steady-state current (I_{SS}) *versus* the glucose concentration, obtained in the chronoamperometry experiments (Figure 6a). The apparent Michaelis–Menten constant (K_m) can be obtained from the inverse of the intercept in the *x*-axis and represents the affinity of the enzyme for the substrate.[49] From the plots in Figure 6b, the K_m value determined for the GOx-DMIm is 9.3 mM. The K_m values were found to be significantly reduced to 3.4 and 5.1 mM, respectively, for the GOx-DMIm-Au_{25} with GOx fractions of 0.15 and 0.45. The smaller K_m values for the enzymatic reactions indicate that the ionic liquid films containing Au_{25} have higher enzymatic affinity to glucose. It is also noteworthy that the value of 3.4 mM is lower than those determined on different nanoparticle systems.[50−52] The low K_m values and high sensitivity obtained for the GOx-DMIm-Au_{25} composites clearly demonstrate that the Au_{25} ionic liquid acts

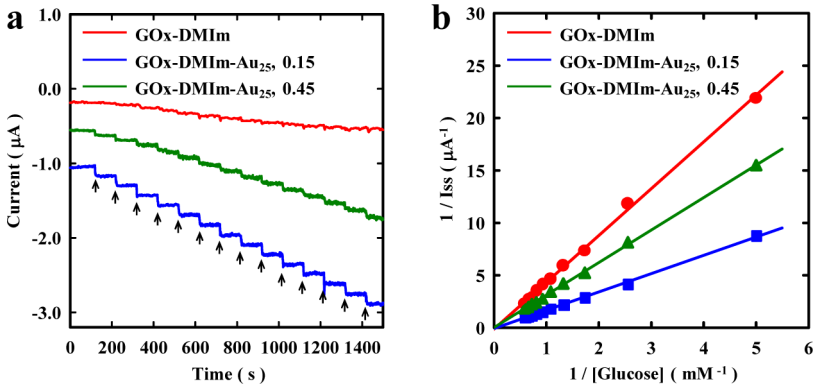

Figure 6. (a) Chronoamperometric current responses of GOx-DMIm (red line) and GOx-DMIm-Au_{25} electrodes with GOx volume fraction of 0.15 (blue line) and 0.45 (green line) to successive addition (with 100 s interval) of 0.2 mM glucose in a stirred PBS (pH 7) containing 0.1 M KCl. The applied potential was 0.31 V *vs* Ag/AgCl. (b) Double reciprocal plots of $1/I_{SS}$ *vs* 1/[glucose] where the steady-state current (I_{SS}) was obtained from the chronoamperometry experiments shown in (a) for GOx-DMIm (red circles) and GOx-DMIm-Au_{25} electrodes with GOx volume fraction of 0.15 (blue squares) and 0.45 (green triangles).

as an excellent support for GOx by presumably providing a favorable microenvironment for the enzymatic reaction.

Fluorescence measurements[53,54] of tryptophan (λ_{ex} = 295 nm) and FAD (λ_{ex} = 370 nm) residues in GOx can be used to monitor the change of its native structure (green line) upon inclusion in the Au_{25} ionic liquid film (red line) and after the glucose sensing experiment (blue line), as shown in Figure S7 (Supporting Information). Whereas the red shift of the tryptophan emission (from 345 to 360 nm) and the additional emission peak of FAD observed at ~600 nm suggest a slight denaturation of the apoenzyme,[54] a large fraction of enzyme (emission at ~520 nm) retains its native conformational state upon inclusion in the ionic liquid film. There is no significant change observed before and after the sensing experiment.

CONCLUSIONS

We have shown that a multifunctioning ionic liquid of a quantum-sized gold cluster can be prepared by ion-pairing of anionic MPS-Au_{25} with imidazolium cations for the first time. Voltammetry study of the Au_{25} ionic liquid film shows that it is electrically conductive, and the electron transport in the film occurs *via* diffusion-like electron hopping process. Composite enzyme electrodes fabricated easily by incorporating GOx in this homogeneous ionic liquid film exhibit excellent mediated electrocatalytic activity that can be successfully exploited for the detection of glucose. The Au_{25} clusters in the composite films act as efficient redox mediators as well as electronic conductors whose transport dynamics was found to control the sensing sensitivity. Furthermore, the composite electrodes were found to be excellent supports for GOx. Quantum-sized gold clusters have shown unique size-dependent redox potentials, electrocatalytic activity, and facile ligand engineering.[16−18] Combined with the unique properties of ionic liquids, these cluster ionic liquids may find important applications not only in biosensors but also in many other electrochemical devices.

MATERIALS AND METHODS

Materials. 1-Decyl-3-methylimidazolium chloride (DMIm-Cl, 96%), glucose oxidase (GOx, EC 1.1.3.4 from *Aspergillus niger*, type X-S, 100−250 units/mg), D-(+)-glucose (>99.5%), potassium chloride (KCl, >99%), tetraoctylammonium bromide (TOABr, 98%), and tetrabutylammonium hexafluorophosphate (Bu_4NPF_6, >99%) were purchased from Sigma-Aldrich. Phosphate buffer solutions (PBS) were prepared from potassium phosphate monobasic (KH_2PO_4, >99%) and potassium phosphate dibasic (K_2HPO_4, >99%). HPLC grade CH_3CN and CH_2Cl_2 were used for electrochemical measurements. All the chemicals and solvents were used as received without further purification. Water was purified using a Millipore Milli-Q system (18.2 MΩ·cm).

Measurements. Electrochemical measurements were performed using an electrochemical workstation CH660B (CH Instruments, Austin, Texas). A conventional three-electrode system comprising a glassy carbon electrode (GCE, 3 mm diameter), DMIm-Au_{25} or GOx-DMIm-Au_{25} electrode as the working electrode, a Pt wire counter electrode and Ag/AgCl (3 M NaCl) reference electrode were used. Voltammetry in nonaqueous solutions was conducted using a platinum working electrode (0.4 mm diameter) and Ag/Ag^+ (0.1 M $AgNO_3$ in CH_3CN) reference electrode. Voltammetry of neat DMIm-Au_{25} films under vacuum was carried out using Ag quasi-reference electrode (AgQRE). UV−vis absorption spectra of MPS-Au_{25} and DMIm-Au_{25} solutions were recorded using a Shimadzu UV−vis−NIR spectrophotometer (UV-3600). Fluorescence measurements of Au_{25} clusters and GOx were conducted using a Symphony InGaAs-1700 spectrofluorometer (Horiba Scientific) and a FS-2 spectrofluorometer (Sinco), respectively. ESI mass spectrometry was performed on a Waters Micromass Q-TOF mass spectrometer. TEM images were collected on a Jeol JEM 2011 microscope. TEM samples were prepared by drop-casting a CH_3CN solution of clusters (1 mg/mL) on a 400 mesh Formvar/carbon-coated copper grid (01814-F, Ted Pella) and drying for 2 h at room temperature before imaging.

Preparation of DMIm-Au_{25} and GOx-DMIm-Au_{25}. Water-soluble MPS-Au_{25} clusters were synthesized according to a procedure described elsewhere.[33] Both DMIm-Au_{25} and GOx-DMIm-Au_{25}

were prepared by ion-pairing with DMIm cations. In a typical procedure, 5 mg of MPS-Au_{25} and 50 mg of 1-decyl-3-methylimidazolium chloride (DMIm-Cl) were dissolved together in 2 mL of 2:1 (v/v) CH_3CN/H_2O in a 10 mL scintillation vial. The solution mixture was stirred vigorously for 10 min for ion-pairing reaction. Upon completion of the reaction, the solution was rotary evaporated to produce highly viscous dark brown product. The product is insoluble in water and CH_2Cl_2 but soluble in CH_3CN. The crude product was subsequently washed with a copious amount of water and then CH_2Cl_2, leaving DMIm-paired Au_{25} ionic liquid (DMIm-Au_{25}). GOx-DMIm-Au_{25} composite was prepared similarly except adding predetermined amount of GOx to the 2 mL of 2:1 (v/v) CH_3CN/H_2O solution. After removing solvents by rotary evaporation, the crude product was thoroughly washed with water and then CH_2Cl_2 to remove unbound GOx and DMIm, respectively. The amount of GOx incorporated into the GOx-DMIm-Au_{25} composite was determined by measuring the concentration of GOx extracted in the aqueous washing solution using fluorescence spectrometry (λ_{EX} = 370 nm and λ_{EM} = 535 nm).

Fabrication of DMIm-Au_{25}- and GOx-DMIm-Au_{25}-Modified Electrodes. DMIm-Au_{25}- and GOx-DMIm-Au_{25}-modified electrodes were prepared by drop-casting 5 μL CH_3CN solutions of DMIm-Au_{25} and GOx-DMIm-Au_{25} composites on the surface of a GCE, respectively, followed by drying overnight in a refrigerator (below −4 °C). DMIm-Au_{25}- and GOx-DMIm-Au_{25}-modified electrodes thus obtained were subsequently rinsed with water, and then their electrochemical behavior and electrocatalytic activity were investigated at room temperature. A representative photograph of DMIm-Au_{25}-modified electrodes is shown in Figure S8 (Supporting Information). The volume fraction of GOx in the GOx-DMIm-Au_{25} film was estimated by measuring the volume (area × thickness) of the composite film drop-cast on a glass substrate. The thickness of the DMIm-Au_{25} film was measured using a surface profilometer (Alpha Step 500, KLA-Tenco) and was typically ~40 μm with a surface roughness less than 10%.

In Figure 5a, electronic diffusion coefficients (D) in the DMIm-Au_{25} and GOx-DMIm-Au_{25} films were determined from CVs obtained at varying scan rates (5−100 mV s^{-1}). Diffusion coefficients were determined from the I_p *versus* $\nu^{1/2}$ slope using the Randles−Sevcik equation.[55]

$$I_p = (2.69 \times 10^5) n^{3/2} A C D^{1/2} \nu^{1/2}$$

where I_p is the peak current, ν is the scan rate, n is the number of electrons transferred, A is the electrode area, and C is the concentration.

Conflict of Interest: The authors declare no competing financial interest.

Acknowledgment. This research was supported by Mid-Career Researcher Program (NRF-2011-0029735), Basic Science Research Program (NRF-2010-0009244), World Class University Program (R32-102170), and Priority Research Centers Program (20110022975) through the National Research Foundation of Korea (NRF) funded by the Ministry of Education, Science and Technology, and Yonsei University Research Fund.

Supporting Information Available: Supplementary data for DMIm-Au_{25} clusters and GOx-DMIm-Au_{25} composite electrodes. This material is available free of charge *via* the Internet at http://pubs.acs.org.

REFERENCES AND NOTES

1. Armand, M.; Endres, F.; MacFarlane, D. R.; Ohno, H.; Scrosati, B. Ionic-Liquid Materials for the Electrochemical Challenges of the Future. *Nat. Mater.* **2009**, *8*, 621–629.
2. Lodge, T. P. A Unique Platform for Materials Design. *Science* **2008**, *321*, 50–51.
3. Singh, V. V.; Nigam, A. K.; Batra, A.; Boopathi, M.; Singh, B.; Vijayaraghavan, R. Applications of Ionic Liquids in Electrochemical Sensors and Biosensors. *Int. J. Electrochem. Sci.* **2012**, *2012*, 1–19.
4. Shiddiky, M. J. A.; Torriero, A. A. J. Application of Ionic Liquids in Electrochemical Sensing Systems. *Biosens. Bioelectron.* **2011**, *26*, 1775–1787.
5. Kim, M. H.; An, S.; Won, K.; Kim, H. J.; Lee, S. H. Entrapment of Enzymes into Cellulose−Biopolymer Composite Hydrogel Beads Using Biocompatible Ionic Liquid. *J. Mol. Catal. B* **2012**, *75*, 68–72.
6. Sato, T.; Masuda, G.; Takagi, K. Electrochemical Properties of Novel Ionic Liquids for Electric Double Layer Capacitor Applications. *Electrochim. Acta* **2004**, *49*, 3603–3611.
7. Heller, A. Electrical Wiring of Redox Enzymes. *Acc. Chem. Res.* **1990**, *23*, 128–134.
8. Wu, X.; Zhao, B.; Wu, P.; Zhang, H.; Cai, C. Effects of Ionic Liquids on Enzymatic Catalysis of the Glucose Oxidase toward the Oxidation of Glucose. *J. Phys. Chem. B: Enzym.* **2009**, *113*, 13365–13373.
9. Vostiar, I.; Ferapontova, E. E.; Gorton, L. Electrical "Wiring" of Viable Gluconobacter Oxydans Cells with a Flexible Osmium-Redox Polyelectrolyte. *Electrochem. Commun.* **2004**, *6*, 621–626.
10. Pauliukaite, R.; Doherty, A. P.; Murnaghan, K. D.; Brett, C. M. A. Application of Some Room Temperature Ionic Liquids in the Development of Biosensors at Carbon Film Electrodes. *Electroanalysis* **2008**, *20*, 485–490.
11. Yang, F.; Jiao, L.; Shen, Y.; Xu, X.; Zhang, Y.; Niu, L. Enhanced Response Induced by Polyelectrolyte-Functionalizedionic Liquid in Glucose Biosensor Based on Sol−Gel Organic−Inorganic Hybrid Material. *J. Electroanal. Chem.* **2007**, *608*, 78–83.
12. Patolsky, F.; Weizmann, Y.; Willner, I. Long-Range Electrical Contacting of Redox Enzymes by SWCNT Connectors. *Angew. Chem., Int. Ed.* **2004**, *43*, 2113–2117.
13. Lee, S.; Ringstrand, B. S.; Stone, D. A.; Firestone, M. A. Electrochemical Activity of Glucose Oxidase on a Poly(ionic liquid)−Au Nanoparticle Composite. *ACS Appl. Mater. Interfaces* **2012**, *4*, 2311–2317.
14. Siedlecka, E. M.; Czerwicka, M.; Stolte, S.; Stepnowski, P. Stability of Ionic Liquids in Application Conditions. *Curr. Org. Chem.* **2011**, *15*, 1974–1991.
15. Toghill, K. E.; Compton, R. G. Electrochemical Non-enzymatic Glucose Sensors a Perspective and an Evaluation. *Int. J. Electrochem. Sci.* **2010**, *5*, 1246–1301.
16. Murray, R. W. Nanoelectrochemistry: Metal Nanoparticles, Nanoelectrodes, and Nanopores. *Chem. Rev.* **2008**, *108*, 2688–2720.
17. Jin, R. Quantum Sized, Thiolate-Protected Gold Nanoclusters. *Nanoscale* **2010**, *2*, 343–362.
18. Maity, P.; Xie, S.; Yamauchi, M.; Tsukuda, T. Stabilized Gold Clusters: From Isolation toward Controlled Synthesis. *Nanoscale* **2012**, *4*, 4027–4037.
19. Nimmala, P. R.; Yoon, B.; Whetten, R. L.; Landman, U.; Dass, A. $Au_{67}(SR)_{35}$ Nanomolecules: Characteristic Size-Specific Optical, Electrochemical, Structural Properties and First-Principles Theoretical Analysis. *J. Phys. Chem. A* **2013**, *117*, 504–517.
20. Walter, M.; Akola, J.; Lopez-Acevedo, O.; Jadzinsky, P. D.; Calero, G.; Ackerson, C. J.; Whetten, R. L.; Grönbeck, H.; Häkkinen, H. A Unified View of Ligand-Protected Gold Clusters as Superatom Complexes. *Proc. Natl. Acad. Sci. U.S.A.* **2008**, *105*, 9157–9162.
21. Lee, D.; Donkers, R. L.; Wang, G.; Harper, A. S.; Murray, R. W. Electrochemistry and Optical Absorbance and Luminescence of Molecule-like Au_{38} Nanoparticles. *J. Am. Chem. Soc.* **2004**, *126*, 6193–6199.
22. Lee, J.; Shim, H. S.; Lee, M.; Song, J. K.; Lee, D. Size-Controlled Electron Transfer and Photocatalytic Activity of ZnO−Au Nanoparticle Composites. *J. Phys. Chem. Lett.* **2011**, *2*, 2840–2845.
23. Jin, R.; Zhu, Y.; Qian, H. Quantum-Sized Gold Nanoclusters: Bridging the Gap between Organometallics and Nanocrystals. *Chem.—Eur. J.* **2011**, *17*, 6584–6593.
24. Varnavski, O.; Ramakrishna, G.; Kim, J.; Lee, D.; Goodson, T. Critical Size for the Observation of Quantum Confinement in Optically Excited Gold Clusters. *J. Am. Chem. Soc.* **2010**, *132*, 16–17.

25. Wu, Z.; Chen, J.; Jin, R. One-Pot Synthesis of $Au_{25}(SG)_{18}$ 2- and 4-nm Gold Nanoparticles and Comparison of Their Size-Dependent Properties. *Adv. Funct. Mater.* **2011**, *21*, 177–183.
26. Lopez-Acevedo, O.; Kacprzak, K. A.; Akola, J.; Häkkinen, H. Quantum Size Effects in Ambient CO Oxidation Catalysed by Ligand-Protected Gold Clusters. *Nat. Chem.* **2010**, *2*, 329–334.
27. Kumar, S. S.; Kwak, K.; Lee, D. Electrochemical Sensing Using Quantum-Sized Gold Nanoparticles. *Anal. Chem.* **2011**, *83*, 3244–3247.
28. Kwak, K.; Kumar, S. S.; Lee, D. Selective Determination of Dopamine Using Quantum-Sized Gold Nanoparticles Protected with Charge Selective Ligands. *Nanoscale* **2012**, *4*, 4240–4246.
29. Lee, D.; Donkers, R. L.; DeSimone, J. M.; Murray, R. W. Voltammetry and Electron-Transfer Dynamics in a Molecular Melt of a 1.2 nm Metal Quantum Dot. *J. Am. Chem. Soc.* **2003**, *125*, 1182–1183.
30. Majda, M. *Molecular Design of Electrode Surfaces*; Murray, R. W., Ed.; Wiley: New York, 1992; pp 159−206.
31. Wang, J. Electrochemical Glucose Biosensors. *Chem. Rev.* **2008**, *108*, 814–825.
32. Heller, A.; Feldman, B. Electrochemical Glucose Sensors and Their Applications in Diabetes Management. *Chem. Rev.* **2008**, *108*, 2482–2505.
33. Kwak, K.; Lee, D. Electrochemical Characterization of Water-Soluble Au_{25} Nanoclusters Enabled by Phase-Transfer Reaction. *J. Phys. Chem. Lett.* **2012**, *3*, 2476–2481.
34. Zhu, M.; Aikens, C. M.; Hollander, F. J.; Schatz, G. C.; Jin, R. Correlating the Crystal Structure of a Thiol-Protected Au_{25} Cluster and Optical Properties. *J. Am. Chem. Soc.* **2008**, *130*, 5883–5885.
35. Negishi, Y.; Nobusada, K.; Tsukuda, T. Glutathione-Protected Gold Clusters Revisited: Bridging the Gap between Gold(I)−Thiolate Complexes and Thiolate-Protected Gold Nanocrystals. *J. Am. Chem. Soc.* **2005**, *127*, 5261–5270.
36. Kim, J.; Lema, K.; Ukaigwe, M.; Lee, D. Facile Preparative Route to Alkanethiolate-Coated Au_{38} Nanoparticles: Post-synthesis Core Size Evolution. *Langmuir* **2007**, *23*, 7853–7858.
37. Xiao, Y.; Patolsky, F.; Katz, E.; Hainfeld, J. F.; Willner, I. "Plugging into Enzymes": Nanowiring of Redox Enzymes by a Gold Nanoparticle. *Science* **2003**, *299*, 1877–1881.
38. Holland, J. T.; Lau, C.; Brozik, S.; Atanassov, P.; Banta, S. Engineering of Glucose Oxidase for Direct Electron Transfer *via* Site-Specific Gold Nanoparticle Conjugation. *J. Am. Chem. Soc.* **2011**, *133*, 19262–19265.
39. Baravik, I.; Tel-Vered, R.; Ovits, O.; Willner, I. Electrical Contacting of Redox Enzymes by Means of Oligoaniline-Cross-Linked Enzyme/Carbon Nanotube Composites. *Langmuir* **2009**, *25*, 13978–13983.
40. Pazur, J. H.; Kleppe, K. The Oxidation of Glucose and Related Compounds by Glucose Oxidase from *Aspergillus niger*. *Biochemistry* **1964**, *3*, 578–583.
41. Chitnis, A.; Sadana, A. pH-Dependent Enzyme Deactivation Models. *Biotechnol. Bioeng.* **1989**, *34*, 804–818.
42. Sun, S.; Zhang, X.; Sun, Y.; Yang, S.; Song, X.; Yang, Z. Facile Water-Assisted Synthesis of Cupric Oxide Nanourchins and Their Application as Nonenzymatic Glucose Biosensor. *ACS Appl. Mater. Interfaces* **2013**, *5*, 4429–4437.
43. Guo, C. X.; Sheng, Z. M.; Shen, Y. Q.; Dong, Z. L.; Li, C. M. Thin-Walled Graphitic Nanocages as a Unique Platform for Amperometric Glucose Biosensor. *ACS Appl. Mater. Interfaces* **2010**, *2*, 2481–2484.
44. Qiu, J.-D.; Wang, R.; Liang, R.-P.; Xia, X.-H. Electrochemically Deposited Nanocomposite Film of Cs-Fc/Au NPs/GOx for Glucose Biosensor Application. *Biosens. Bioelectron.* **2009**, *24*, 2920–2925.
45. Bauhofer, W.; Kovacs, J. Z. A Review and Analysis of Electrical Percolation in Carbon Nanotube Polymer Composites. *Compos. Sci. Technol.* **2009**, *69*, 1486–1498.
46. Last, B. J.; Thouless, D. J. Percolation Theory and Electrical Conductivity. *Phys. Rev. Lett.* **1971**, *27*, 1719–1721.
47. Kachoosangi, R. T.; Musameh, M. M.; Abu-Yousef, I.; Yousef, J. M.; Kanan, S. M.; Xiao, L.; Davies, S. G.; Russell, A.; Compton, R. G. Carbon Nanotube−Ionic Liquid Composite Sensors and Biosensors. *Anal. Chem.* **2009**, *81*, 435–442.
48. Liu, Y.; Liu, L.; Dong, S. Electrochemical Characteristics of Glucose Oxidase Adsorbed at Carbon Nanotubes Modified Electrode with Ionic Liquid as Binder. *Electroanalysis* **2007**, *19*, 55–59.
49. Thévenot, D. R.; Toth, K.; Durst, R. A.; Wilson, G. S. Electrochemical Biosensors Recommended Definitions and Classification. *Biosens. Bioelectron.* **2001**, *16*, 121–131.
50. Pandey, P.; Singh, S. P.; Arya, S. K.; Gupta, V.; Datta, M.; Singh, S.; Malhotra, B. D. Application of Thiolated Gold Nanoparticles for the Enhancement of Glucose Oxidase Activity. *Langmuir* **2007**, *23*, 3333–3337.
51. Wan, D.; Yuan, S.; Li, G. L.; Neoh, K. G.; Kang, E. T. Glucose Biosensor from Covalent Immobilization of Chitosan-Coupled Carbon Nanotubes on Polyaniline-Modified Gold Electrode. *ACS Appl. Mater. Interfaces* **2010**, *2*, 3083–3091.
52. Wu, B.-Y.; Hou, S.-H.; Yin, F.; Li, J.; Zhao, Z.-X.; Huang, J.-D.; Chen, Q. Amperometric Glucose Biosensor Based on Layer-by-Layer Assembly of Multilayer Films Composed of Chitosan, Gold Nanoparticles and Glucose Oxidase Modified Pt Electrode. *Biosens. Bioelectron.* **2007**, *22*, 838–844.
53. Gooding, J. J.; Situmorang, M.; Erokhin, P.; Hibbert, D. B. An Assay for the Determination of the Amount of Glucose Oxidase Immobilised in an Enzyme Electrode. *Anal. Commun.* **1999**, *36*, 225–228.
54. Przybyt, M. Behaviour of Glucose Oxidase during Formation and Ageing of Silica Gel Studied by Fluorescence Spectroscopy. *Mater. Sci* **2003**, *21*, 397–416.
55. Bard, A. J.; Faulkner, L. R. *Electrochemical Methods: Fundamentals and Applications*, 2nd ed.; John Wiley & Sons: New York, 2001.